Nuclear-reactor pumped lasers excited by ion-ion neutralization[a)]

M. J. Kushner
Lawrence Livermore National Laboratory, P. O. Box 808, Livermore, California 94550

(Received 26 April 1982; accepted for publication 23 September 1982)

A class of nuclear pumped lasers (excited by reactor-produced thermal neutrons) in which the laser levels are populated by negative ion-positive ion neutralization is proposed and an analysis of two particular systems, $^3He/N_2O/O_2$ and $^3He/N_2O/N_2$, is performed. Laser action is predicted in atomic oxygen and nitrogen as a result of O^--O^+ and O^--N^+ neutralizations. The source of negative ions is dissociative attachment to N_2O. A threshold neutron flux of $\approx 10^{15} cm^{-2} s^{-1}$, peak power of > 500 W/cm^2, and a fission power to laser power conversion efficiency of $\approx 0.4\%$ may be possible in these systems. This is as a result of efficient utilization of the large thermal electron density in the attachment process, and the highly selective nature of the ion-ion neutralization in producing product-excited states.

PACS numbers: 42.55.Hq, 28.50. − k, 34.90. + q

I. INTRODUCTION

Nuclear pumped lasers (NPL) convert the kinetic energy of fission fragments into coherent laser light.[1–5] A typical NPL is a gas laser with a large partial pressure of a fissile gas (e.g., ^3He) and a small partial pressure of the lasant gas. In the presence of an externally generated thermal neutron flux, the fissile gas absorbs a neutron and fissions, releasing hundreds of keV to hundreds of MeV of energy primarily as the kinetic energy of the fission fragments. The fission fragments slow down by ionizing the gas, producing a distribution of high-energy primary electrons. The primary electrons in turn slow down by exciting and ionizing the gas, producing a secondary electron distribution. An inversion is the direct or indirect product of the secondary electrons.

A number of nuclear pumped lasers have been reported and have successfully demonstrated the scalability of such systems.[1–5] Nuclear pumped lasers are attractive because the mean free path of a neutron through a fissile gas can be many centimeters long so large volumes of gas can be uniformly pumped. Although the NPL reported to date have shown a great deal of promise, laser energy and power have been relatively low. The reasons for this are twofold. First, a neutron-generating system has not been built specifically for use as an NPL, although numerous designs have been proposed.[6] The coupling of the neutron source to the laser has therefore been poor. Secondly, the electron distribution in an NPL is not conducive to directly exciting the laser levels and producing an inversion. Therefore an indirect method (e.g., charge exchange and/or recombination) must be relied on to produce the inversion.[7,8]

The electron distribution function in a nuclear pumped plasma consists of a high-energy tail and a large thermal group.[9,10] The high-energy tail is a result of the primary electrons. Since there is no upflux (i.e., applied electric field), the primary and secondary electrons slow down rapidly, cascading to lower energies until they accumulate in a large thermal group. The high-energy tail and epithermal electrons are responsible for exciting and ionizing the gas. The thermal group, below any excitation threshold, contains the majority of the electrons. They cannot directly excite the gas, but do recombine rapidly. In an electron-ion recombination, the recombining electron occupies a level within a few kT of the continuum. An inversion is produced if while the electron cascades through the atomic levels to the ground state, a bottleneck occurs at a long-lived state. Because the recombination does not directly populate the upper laser level, it is not a very selective process, and efficiency suffers as a result.

In order to design a more efficient NPL, one must be able to use the large thermal electron density in a selective excitation process. In this paper, a method is proposed whereby this goal is met, and an analysis is performed for a nuclear pumped laser whose excitation mechanism is negative ion-positive ion neutralization. For the system proposed, the attachment process, which produces the negative ions, is largest for thermal electrons. The ion-ion recombination is highly selective in terms of the states of the product neutral atoms which are populated.[11,12] The result is a relatively efficient laser ($\approx 0.4\%$). The specific laser systems proposed consist of mixtures of $^3He/O_2/N_2O$ and $^3He/N_2/N_2O$. Laser action in atomic oxygen and nitrogen occurs as a result of O^--O^+ and O^--N^+ neutralizations. The nuclear pumping reaction is

$$n + {}^3He \rightarrow p + {}^3H + 760 \text{ keV}. \quad (1)$$

The thermal fission cross section is 5280×10^{-24} cm^2. 760 keV of kinetic energy is released, mostly in the proton. Negative ions are formed by the dissociative attachment reaction

$$e + N_2O \rightarrow N_2 + O^-. \quad (2)$$

The magnitude of the cross section for this reaction depends both on the electron energy and gas temperature.[13,14]

Although only these specific systems will be discussed, many negative ion-positive ion pairs may produce inversions by rapid neutralization. Ion-ion neutralization has been proposed as an excitation source in atomic lasers,[15] although experimental results for such a system have not been reported. Ion-ion neutralization is thought to play an important role for the formation of exciplexes in excimer laser systems.[16]

The theory of ion-ion neutralization will be discussed in

[a)] This work performed under the auspices of the U.S. Department of Energy by the Lawrence Livermore National Laboratory under Contract Number W-7405-ENG-78.

 0021-8979/83/010039-09$02.40

Sec. II followed by a description of the model system in Secs. III and IV. A parametric study contrasting the $^3He/N_2O/O_2$ and $^3He/N_2O/N_2$ laser systems will be presented in Sec. V.

II. THEORY OF ION-ION NEUTRALIZATION

The selectivity of the ion-ion neutralization process in terms of the product states can be explained by referring to Fig. 1 where a typical potential energy diagram for the collision and neutralization of a negative ion-positive ion pair is displayed. For the separations of interest here, the incoming ion pair approach with coulomb potential, while the neutral product pair have a constant intra-atomic potential. The curve crossing responsible for the recombination occurs over a limited energy and therefore accesses only a limited number of product states. The width of the resonance is a few tenths of an eV.

The ion-ion neutralization process for atomic species is well described by the Landau-Zener theory. The specifics of that theory as pertains to ion-ion neutralization is described in detail in Refs. 11 and 12. The theory will be briefly described below.

For ions in their ground state and at large separations, the interatomic potential is coulombic. That is,

$$V_i(R) = \langle i|H|i\rangle = \frac{-e^2}{R}. \tag{3}$$

The neutral products have a constant potential at large separations

$$V_f^0(R) = \langle f|H|f\rangle = -[I(X^*) - EA(Y^*)] = -\Delta E, \tag{4}$$

where I and EA are the ionization potential and electron affinity of the (excited) products. By large separation, we mean that

$$\frac{\sigma_{LJ}}{R^6} \ll \frac{e^2}{R}, \tag{5}$$

where σ_{LJ} is the interatomic Lennard-Jones potential. The curve crossing occurs at R_x where $V_i^0(R_x) = V_f^0(R_x)$. That is,

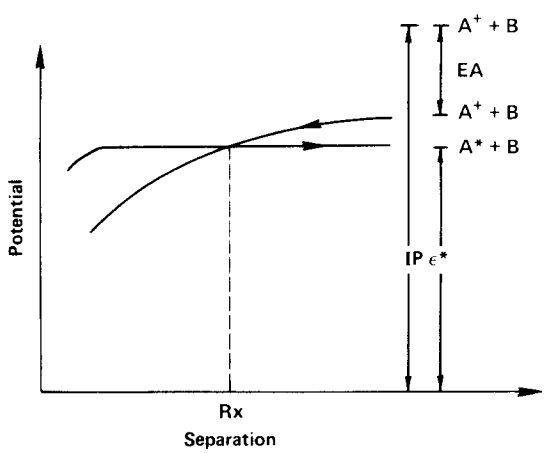

FIG. 1. Potential energy level diagram for the neutralization of A^+ (with ionization potential IP) and B^- (with electron affinity EA). Atom A emerges from the collision at separation R_x excited with energy ϵ^*.

$$R_x = \frac{e^2}{\Delta E}. \tag{6}$$

The probability for a transition between two adiabatic states of ionic and covalent nature is

$$P = 2P_{if}(1 - P_{if}), \tag{7}$$

where P_{if} is the transfer probability at the curve crossing. The factor of 2 accounts for the incoming and outgoing legs. The Landau-Zener probability for the transition is

$$P_{if} = \exp\left(\frac{-2V_x}{V_l}\right), \tag{8}$$

where V_l is the radial velocity for angular momentum l at the curve crossing R_x, and

$$V_x = \frac{2\pi R_x^2}{\hbar e^2}|H_{if}|^2. \tag{9}$$

It can be shown that

$$P_{if} = \exp\left\{-2\left(\frac{2\pi R_x^2}{\hbar e^2}\right)|H_{if}|^2 \Big/ \left[v_l\left(1 + \frac{e^2}{R_x^2 E} - \frac{\rho^2}{E^2}\right)\right]\right\}. \tag{10}$$

The total ion-ion neutralization cross section Q is obtained by integrating over all possible angular momenta.

$$Q = 4\int_0^{\rho_{max}} P_{if}(1 - P_{if})\rho d\rho. \tag{11}$$

The problem reduces to calculating H_{ij}. Olson *et al.*[12] have derived a semiemperical expression for H_{ij} requiring knowledge only of R_x and $\gamma^2/2$, the binding energy of the negative ion. Their expression is

$$H_{ij} = \frac{\gamma^2}{2}[8.0\exp(-0.91\gamma R_x) - 7.5 \times \exp(-0.99\gamma R_x)]. \tag{12}$$

With this form for H_{if}, the integral (11) can be done in closed form.

An example of a calculation for the neutralization cross section between O^- and N^+ as a function of ΔE is shown in Fig. 2. If we assume that the oxygen emerges from the neutralization in the ground state, ΔE is the excitation energy of the product N^*. Note the resonant character of the neutralization cross section. This accounts for the selectivity of product-excited states for the reaction. The probability P_{if} is a function of E and hence gas temperature. In general, the cross section decreases as the incident energy E (and gas temperature) increases.

III. DESCRIPTION OF THE ELECTRON DISTRIBUTION FUNCTIONS

It has been shown that the electron distribution to an NPL is non-Maxwellian,[9,10] and can be described by a high-energy group of electrons and a thermal group of electrons. The electron distribution is described here by combining three groups of electrons, one thermal and two high energy. The first distribution consists of the primary electrons produced by the fission fragments. This group is described by

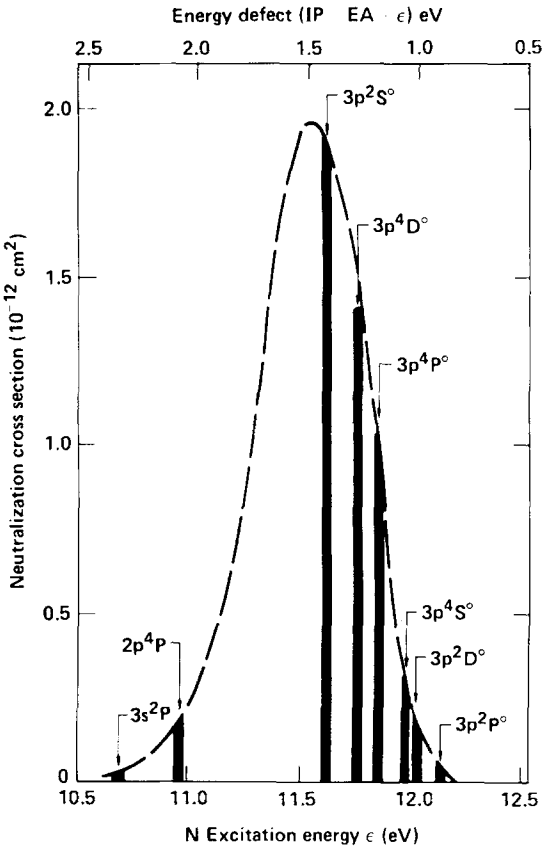

FIG. 2. Calculated cross section for the neutralization of N^+ and O^- showing the excited states in neutral nitrogen which result from the reaction.

the electron distribution $f_1(\epsilon)$ and is calculated in the manner described below. The first group of electrons acts as the source for the second group of electrons (slowed primary and secondary electrons) described by the electron distribution $f_2(\epsilon)$ and will also be discussed below. The third group consists of thermal electrons which have slowed below all inelastic thresholds and are in thermal equilibrium with the buffer gas. These electrons are described by $f_3(\epsilon)$. Because the exciting neutron pulse is relatively long (tens of microseconds to tens of milliseconds), and the gas pressure is large (hundreds of Torr), each distribution $f_i(\epsilon)$ can be considered in a quasi-steady state.

The distribution of primary electrons $f_1(\epsilon)$ is obtained as a by-product of calculating the slowing down spectrum of the fission fragments. In the pumping reactions [Eq. (1)], 760 keV of energy are released as kinetic energy of the proton and triton. For simplicity, assume that all of the fission energy is released in the form of monoenergetic 760-keV protons. The distribution of protons which result from the slowing down of 760-keV fission fragments is $F_p(T)$ (cm^3 eV s)$^{-1}$, where

$$\frac{dF_p(T)}{dt} = -F_p(T)\left(\frac{2T}{M}\right)^{1/2}\sum_{i,j} N_i \int_{E_{ij}}^{T}\sigma_{ij}(T,\epsilon)d\epsilon + \sum_{i,j} N_i \int_{E_{ij}}^{T_{\max}-T} F_p(T+\epsilon)\left(\frac{2(T+\epsilon)}{M}\right)^{1/2} \times \sigma_{ij}(T+\epsilon,\epsilon)d\epsilon + N_f\Phi_n\sigma_f(T). \quad (13)$$

In Eq. (13), $\sigma_{ij}(T,\epsilon)$ is the cross section for a proton of energy T exciting species i by process j while losing energy ϵ. N_i is the density of species i, E_{ij} is the threshold energy for process j, species i; $T_{\max}$ is the maximum fission fragment energy, and M is the fission fragment mass. N_f is the fissile atom density, Φ_n is the thermal neutron flux, and $\sigma_f(T)$ is the fission cross section for producing a fission fragment of energy T (cm^2/ev). The first term of Eq. (17) is due to losses out of $F_p(T)$ by collisions. The second term is due to contributions to $F_p(T)$ from fission fragments slowing down with energy greater than T, and the third term is the source function for $F_p(T)$ as a result of fissions. For our purposes, $\sigma_f(T) = \sigma_f\delta(T - T_{\max})$. In the quasi-steady state,

$$F_p(T) = \frac{\sum_{i,j} N_i \int_{E_{ij}}^{T_{\max}-T}\left(\frac{2(T+\epsilon)}{M}\right)^{1/2} F_p(T+\epsilon)\sigma_{ij}(T+\epsilon,\epsilon)d\epsilon + N_f\Phi_n\sigma_f(T)}{\left(\frac{2T}{M}\right)^{1/2}\sum_{i,j} N_i \int_{E_{ij}}^{T}\sigma_{ij}(T,\epsilon)d\epsilon}. \quad (14)$$

Once $F_p(T)$ is calculated, the primary electron spectrum $f_1(\epsilon)$ is obtained by integrating the differential slowing down cross section for ionizations:

$$f_1(\epsilon) = \Sigma_{i,j} N_i \int_{\epsilon + E_{ij}^I}^{T_{\max}} F_p(T)\sigma_{ij}^I(T,\epsilon + E_{ij}^i)dT, \quad (15)$$

where σ_{ij}^I is the differential cross section for ionization of species i by process j, and E_{ij}^I is the ionization potential. The differential cross sections $\sigma_{ij}^I(T,\epsilon)$ were taken from Ref. 17 for the case of ionization and excitation by heavy particles.

The distribution function $f_2(\epsilon)$ is next calculated with $f_1(\epsilon)$ serving as the source function. The calculation of $f_2(\epsilon)$ was performed by solving the Boltzmann equation in finite difference form using the program described in Ref. 18. For other detailed descriptions of the method, see Refs. 19 and 20. In solutions of the Boltzmann equation in electric discharges, low threshold events, especially resonant types of collisions such as vibrational excitation, are particularly important. This is due to the fact that the source of energetic electrons are thermal electrons which are accelerated by the electric field. This is sometimes called the electron upflux. Only electrons which suffer very few low threshold, nonionizing collisions become energetic enough to cause ionizations. As a result, in an electric discharge the majority of ionizations are due to electrons which just reach the threshold energy so to a very good approximation, secondary elec-

trons can be assumed to be born with thermal or zero energy.

In a nuclear (*e*-beam or proton beam) pumped plasma and in the absence of an applied electric field, there is no upflux. Ignoring superelastic and *e-e* collisions, electrons can only slow down. Therefore collisions whose cross sections are only large below the smallest ionization threshold (such as vibrational excitation and resonant electronic excitation) have little or no effect on the total ionization rate. In addition, the majority of ionizations are by electrons whose energy is significantly larger than the threshold value. Therefore in calculating $f_2(\epsilon)$, one must specify a distribution of secondary electrons which result from an electron impact ionization.

The form of the cross section for secondary electrons resulting from electron impact ionization was taken from the work of Opal *et al.*[21] Using the fitting functions of Green and Sawada,[22] the cross section for producing a secondary electron of energy T by a primary electron of energy E is $S(E,T)$ cm^2/eV, where

$$S(E,T) = A(E)\frac{\Gamma^2}{(T-T_0)^2+\Gamma^2}, \tag{16}$$

and

$$A(E) = \sigma_0 \frac{K}{E} \ln\frac{E}{J}, \tag{17a}$$

$$\Gamma = \Gamma_s \frac{E}{E+\Gamma_b}, \tag{17b}$$

$$T_0 = T_s - \frac{T_a}{E+T_b}. \tag{17c}$$

The parameters K, J, Γ_s, T_s, T_a, and T_b are tabulated in Ref. 22 for various gases.

In the absence of an applied electric field and superelastic collisions, electrons which slow down below the lowest excitation threshold continue to slow down by elastic collisions. These electrons eventually become thermalized and can be described by a Maxwellian distribution with the gas temperature T_g, $f_3(\epsilon)$. The rate of transfer from $f_2(\epsilon)$ to $f_3(\epsilon)$ is therefore the elastic collision frequency. Although $f_3(\epsilon)$ contains electrons which are below any excitation threshold, recombination events and certain attachment processes are important for this group. The rate of these processes usually vary with some power of the inverse of the electron temperature. Therefore, recombination occurs almost exclusively out of the thermal group. Since recombination and attachment are in general slow compared to the rate at which electrons slow down to join $f_3(\epsilon)$ (especially at high pressure, where diffusion as a loss mechanism can be ignored), the density of electrons in $f_3(\epsilon)$ is almost always large compared to the density of electrons in $f_1(\epsilon)$ and $f_2(\epsilon)$. A sample of the calculated primary electron distribution for ^{3}He/N_2 gas mixtures is shown in Fig. 3. The combined distributions $f_1(\epsilon)$ and $f_2(\epsilon)$ for the same conditions are shown in Fig. 4. The first cutoff near 10 eV is due to electronic excitation of N_2, while the cutoff near 15 eV is due to ionization of N_2. The electrons with higher energy than the 25-eV cutoff from ionization of ground state helium are due mainly to primary

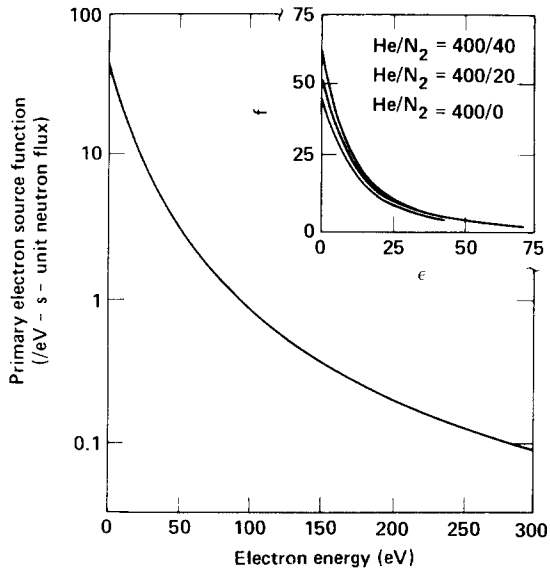

FIG. 3. Primary electron spectrum resulting from ionization by fission fragments P as calculated with Eq. (14) for mixtures of He and N_2. The helium number density is 1.3×10^{19} cm^{-3}. The inset shows the distribution for low electron energy.

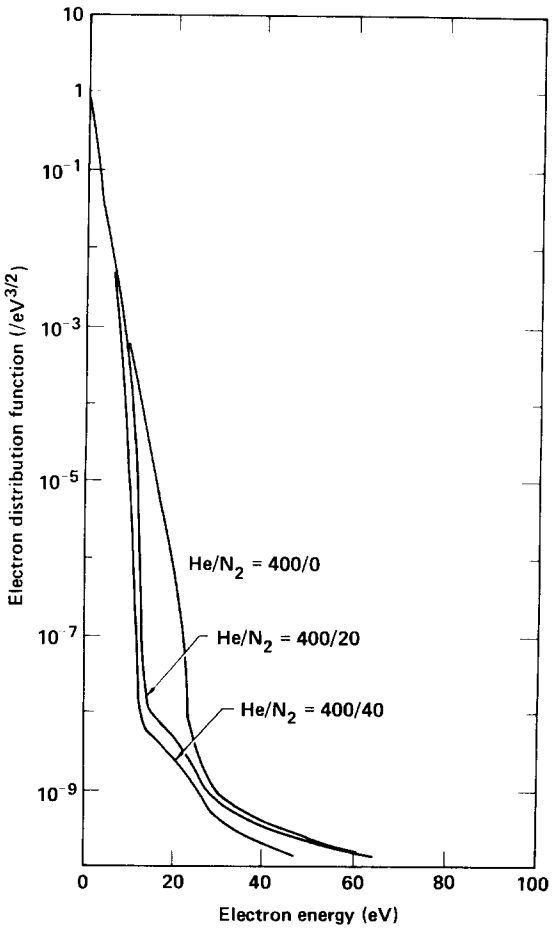

FIG. 4. Primary and secondary electron distribution function for mixtures of He and N_2 for the conditions of Fig. 3.

electrons and primary electrons which have undergone only a few collisions.

IV. DESCRIPTION OF THE MODEL LASER SYSTEM

Given the large density of thermal electrons, an ion-ion recombination laser is only feasible if the attachment process is largest for thermal electrons. This eliminates most dissociative attachment processes (e.g., O_2, H_2O, CO_2) which have thresholds of a few eV.[23] Processes which meet this requirement are attachment to SF_6,[24] and dissociation attachment of F_2,[25] and N_2O.[13,14] We shall limit our discussions to the latter, a process which efficiently produces O^- ions.

At room temperature, the dissociative attachment of N_2O has a small cross section with a threshold value of a few tenths of an eV.[13] The process, though, has an additional activation energy which can be satisfied by the internal degrees of freedom of the N_2O molecule. The result is that the reaction (2) has an electron impact cross section for $\epsilon < 2$ eV which increases exponentially with increasing gas temperature. For gas temperatures less than 400 °K, this activation energy is about 0.23 eV. For temperatures above 400 °K, the activation energy is smaller.[14] Assuming that the electrons are in thermal equilibrium with the N_2O gas, the rate of dissociative electron attachment as a function of gas temperature is shown in Fig. 5. N_2O is primarily consumed by the dissociative attachment reaction (2). Other electron impact processes produce atomic oxygen and nitrogen. Various chemical reactions occur which result in producing large amounts of NO at the expense of N_2O. A list of the chemical reactions and other species considered for the system are in Tables I and II.

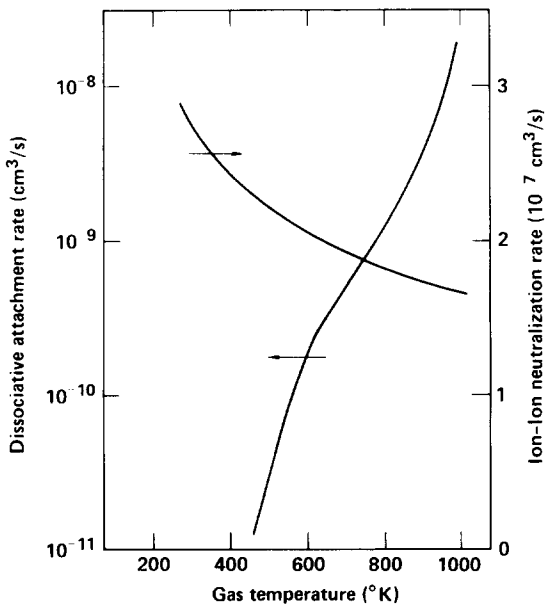

FIG. 5. Dissociative attachment rate of electrons to N_2O as a function of gas temperature. The electrons were assumed to have a Maxwellian distribution with the same temperature. Also shown is the ion-ion neutralization rate for O^+ and O^-. The pumping rate [(attachment rate)×(neutralization rate)] increases with increasing gas temperature.

TABLE I. Species included in the model.

Ground states:	O	N	He	N_2O
	O_2	N_2		NO
	O_3			NO_2
Excited states:	O*	$3p^3P$, $3s^3S^0$		
	N*	$3p^4S^0$, $3p^4P^0$, $3s^4P$, $3p^4D^0$, $3s^2P$, $3p^2D^0$, $3p^2S^0$		
	He*	2^3S_1		
Charged species:	N^+	O^+	He^+	O^-
	N_2^+	O_2^+	He_2^+	e^a
	N_3^+	O_4^+	N_2O^+	e_T^b
	N_4^+			

[a] Nonthermal electrons (groups 1 and 2).
[b] Thermal electrons (group 3).

The electron impact processes, neutral and ion collisions included in the analysis are listed in Tables II and III. Separate electron densities were calculated for the thermal group and groups f_2 and f_3. Electrons in the latter two groups can participate in all processes except dissociative attachment and recombination. Electrons in the thermal group can only participate in recombination, attachment, and superelastic relaxation. Because of the high pressure, large dimensions of the system ($\gtrsim 10$ cm), and short neutron pulse ($\lesssim 200$ μs), diffusion can be ignored.

The branching ratios of the ion-ion neutralization process of N^+ and O^- favor the $3p^4S^0$, $3p^4P^0$, and $3p^4D^0$ states in the quartet system, and the $3p^2D^0$ and $3p^2S^0$ states in the doublet system in nitrogen. Gain can be expected for both systems. In the O^+-O^- neutralization, the $3p^3P$ and $3p^5P$

TABLE II. Reactions involving electrons and fission fragments.

Fission fragments (f):

$f + He$	→	$He^* + f$
	→	$He^+ + f$
$f + N_2$	→	$N_2^+ + e + f$
	→	$N^+ + N + e + f$
	→	$2N + f$
$f + O_2$	→	$O_2^+ + e + f$
	→	$O^+ + O + e + f$
	→	$2O + f$

Electron collisions:

$e + M^*$	⇄	$M^{**} + e$	M = He, N_2^a, N, O_2^a, O, N_2O
$e + M$	⇄	$M^+ + 2e$	M = Ne, N_2, N, O_2, O, N_2O
$e + M^+$	→	M	M = He, N_2, N, O_2, O, N_2O
$e + M_2^+$	→	2M	M = He, N, O
$e + M_2$	→	$2M + e$	M = N, O
$e + M_2$	→	$M + M^+ + 2e$	M = N, O
$e + N_3^+$	→	$N_2 + N$	
$e + M_4^+$	→	$2M_2$	M = N, O
$e + N_2O$	→	$N_2 + O + e$	
$e + NO$	→	$N + O + e$	
$e + NO_2$	→	$NO + O + e$	
$e + N_2O$	→	$N_2 + O^-$	
$e + O_2$	→	$O + O^-$	
$e + O$	→	O^-	
$e + O^-$	→	$O + 2e$	

Note: M^{**} is any excited state with a higher energy than M^*.
[a] Only the forward reaction was used in calculation of electron distribution function.

states are the major products, with more than half of the neutralizations populating the $3p^3P$ states. Laser action has been observed on the $3p^2S^0_{1/2}$-$3s^2P_{3/2}$ transition in nitrogen[26] and the $3p^3P_2$-$3s^3S^0_1$ transition in oxygen.[26] The latter transition has shown gain in another nuclear pumped system.[27] These two transitions also have relatively high gain in the systems to be described here.

In addition to those levels discussed above, the $3s^4P$, $2d^4P$, and $3s^2P$ levels in nitrogen and the $3s^3S^0$ level in oxygen, as well as the ground states, were included in the analysis. Since each level is a multiplet with up to four members, the following method was used to calculate the density of atoms in any given multiplet level. The rate equations discussed below were used to calculate the total density for each set of multiplets. Since the multiplet members are closely spaced (the largest spacing between adjacent multiplet members is 43 cm^{-1}) and most processes are quasi-steady state, it was assumed that the multiplet members are in equilibrium with the thermal electron group and the background gas. Therefore, the density of a given multiplet member j of level i is

$$n_{ij} = \frac{N_i g_{ij} \exp(-\epsilon_{ij}/kT)}{\Sigma_{i,l} g_{il} \exp(-\epsilon_{il}/kT)},$$

where N_i is the total density of the level, g_{ij} is the degeneracy of multiplet member (i,j), and ϵ_{ij} is the energy of multiplet member (i,j) measured relative to the lowest lying member in the multiplet.

For the pressures considered here ($\geqslant$400 Torr), all the transitions were assumed to be homogeneously (pressure) broadened. It has been reported that the $3p^3P_2$-$3s^3S^0_1$ transition in oxygen (8446 Å) often lases in the wings of the line.[28] The reason for this behavior is thought to be selective resonance reabsorption. In low-pressure, electric-discharge oxygen lasers, population of the upper laser level is believed to be a result of a dissociative Penning reaction. The excess energy of the reaction appears partly as kinetic energy of the products. Therefore, the upper laser level can be a member of a higher velocity class having a wider Doppler-broadened line than the ground state. This velocity distribution is transferred to the lower laser level during the optical transition. Trapping of radiation from the lower laser level by the ground state, which has a lower temperature and a narrower line profile, preferentially repopulates the lower level near the center of the line. This causes gain to be highest in the wings of the line. In the system discussed here, both the upper laser level and the ground state are members of the same velocity class. Therefore, selective resonance reabsorption does not apply, and lineshape-averaged trapping factors can be used.

Rate equations for the reactions in Tables II and III were formulated and integrated over a Gaussian neutron pulse with a width of 100 μs. Electron impact rates were calculated by averaging the energy dependent cross section over the appropriate distribution function. The gas temperature was specified and assumed to be constant. The laser intensity for the transition between multiplet member k of level j, and member l of level m is

$$\frac{dI^{jk}_{ml}}{dt} = BI^{jk}_{ml}\left[\frac{N_j g_{ml} e^{-\epsilon_{jk}/T}}{\sum_n g_{jn} e^{-\epsilon_{jn}/T}} - \frac{N_m g_{jk} e^{-\epsilon_{ml}/T}}{\sum_n g_{mn} e^{-\epsilon_{mn}/T}}\right] + I^{jk}_{ml} \ln(R_1R_2)c/2L + A^{jk}_{ml}\frac{\beta N_j g_{ml} e^{-\epsilon_{jk}/T}}{\sum_n g_{jn} e^{-\epsilon_{jn}/T}}, \quad (19)$$

where B is the stimulated emission coefficient, R_1 and R_2 are

TABLE III. Reactions between ions and neutral species.

Ion-ion reactions:			
$O^- + M^+$	$\rightarrow$	$M + O$	M = He, N_2, N, O_2, O, N_2O
$O^- + M^+$	$\rightarrow$	$M^* + O$	M = He, N, O
$O^- + M_4^+$	$\rightarrow$	$2M_2 + O$	M = N, O
Ion-neutral reactions:			
$He^+ + NO$	$\rightarrow$	$N^+ + O + He$	
$He^+ + N_2O$	$\rightarrow$	$N_2 + O^+ + He$	
	$\rightarrow$	$N_2^+ + O + He$	
	$\rightarrow$	$NO + N^+ + He$	
$He^+ + M$	$\rightarrow$	$M^+ + He$	M = N_2, O_2, N, O
$He_2^+ + M$	$\rightarrow$	$M^+ + 2He$	M = N_2, N, O_2, O, N_2O
$He_2^+ + M_2$	$\rightarrow$	$M^+ + M + 2He$	M = N
$O_2^+ + O_2 + He$	$\rightleftarrows$	$He + O_4^+$	
$O_2^+ + 2O_2$	$\rightleftarrows$	$O_4^+ + O_2$	
$O_4^+ + O$	$\rightarrow$	$O_2^+ + O_3$	
$N^+ + N_2 + M$	$\rightarrow$	$N_3^+ + M$	M = He, N_2
$N_2^+ + N_2 + M$	$\rightarrow$	$N_4^+ + M$	M = He, N_2
$N^+ + N_2O$	$\rightarrow$	$N_2O^+ + N$	
$N^+ + O_2$	$\rightarrow$	$O^+ + NO$	
	$\rightarrow$	$O_2^+ N$	
$N_2^+ + M$	$\rightarrow$	$M^+ + N_2$	M = N, N_2O, O, O_2
$N_3^+ + M$	$\rightarrow$	$N + N_2 + M^+$	M = N_2O, O_2
$N_4^+ + M$	$\rightarrow$	$2N_2 + M^+$	M = N_2O, O_2
$O^- + N_2O$	$\rightarrow$	$2NO + e$	
$O^- + N_2O$	$\rightarrow$	$2NO + e$	
$O^- + N$	$\rightarrow$	$NO + e$	
$O^- + NO$	$\rightarrow$	$NO_2 + e$	
$O^- + N_2$	$\rightarrow$	$N_2O + e$	
$O^- + O$	$\rightarrow$	$O_2 + e$	
$O^- + O_2$	$\rightarrow$	$O_3 + e$	
Neutral-neutral reactions:			
$He^* + M_2$	$\rightarrow$	$M^+ + M + He$	M = N, O
$He^* + M$	$\rightarrow$	$M^+ + He + e$	M = N_2, O_2, N_2O, He*
$He^* + M_2$	$\rightarrow$	$2M + He$	M = N_2, O_2
$N + N + M$	$\rightleftarrows$	$N_2 + M$	M = He, N_2, O_2, N_2O
$O + O + M$	$\rightleftarrows$	$O_2 + M$	M = He, N_2, O_2, N_2O
$O + O_2 + M$	$\rightleftarrows$	$O_3 + M$	M = He, N_2, O_2, N_2O
$O + N_2O$	$\rightleftarrows$	$2NO$	
$N + NO$	$\rightleftarrows$	$O + N_2$	
$NO_2 + M$	$\rightleftarrows$	$NO + O + M$	M = He, N_2, O_2, N_2O
$O_3 + O_3$	$\rightleftarrows$	$3O_2$	
$N_2 + O_2$	$\rightleftarrows$	$2NO$	
$O + N_2O$	$\rightleftarrows$	$N_2 + O_2$	
$N + N_2O$	$\rightleftarrows$	$NO + N_2$	
$N + NO_2$	$\rightleftarrows$	$N_2O + O$	
$NO + N_2O$	$\rightleftarrows$	$NO_2 + N_2$	
$NO + NO_2$	$\rightleftarrows$	$N_2O + O_2$	
$NO_2 + O$	$\rightleftarrows$	$NO + O_2$	
$NO + O_2$	$\rightleftarrows$	$NO_2 + O$	
$NO_2 + N$	$\rightleftarrows$	$O_2 + N_2$	
$2NO_2$	$\rightleftarrows$	$2NO + O_2$	
$N_2O + M$	$\rightleftarrows$	$N_2 + O + M$	M = All
$O_2 + N$	$\rightleftarrows$	$NO + O$	
$O^{**} + M$	$\rightarrow$	$M + O^*$	M = He, N_2, O
$N^{**} + M$	$\rightarrow$	$M + N^*$	M = He, N_2, O

the mirror reflectivities for a cavity of length L, A_{lm}^{jk} is the spontaneous emission coefficient, and β is a geometrical factor.

V. RESULTS FOR A NUCLEAR-PUMPED ION-ION NEUTRALIZATION LASER

Of the two systems considered, laser action by neutral oxygen in $^3He/N_2O/O_2$ mixtures far exceeds laser action by neutral nitrogen in $^3He/N_2O/N_2$ mixtures under comparable conditions. The systematic behavior of the two lasers is similar, though laser power in the oxygen system is an order of magnitude larger than in the nitrogen system. This is due primarily to two causes. The O^--O^+ neutralization results in more than half of the product atoms emerging in the $3p^3P$ upper laser level of the dominant line. A third emerge in the $3p^5P$ state, which is weakly coupled to the lower laser level ($3s^3S$). In addition, there are only three multiplet members between which this excitation is shared. In contrast, the O^--N^+ neutralization populates more states and does so in a more uniform manner. Almost half of the atoms emerge in the $3s^4P^0$ and $3p^4D$ states, both of which have transitions to common lower levels ($3s^4P$ and $2p^4P$). The excitation is shared between four multiplet members. The strongest nitrogen laser line is in the doublet system between the $3p^2D^0$ upper level and the $3s^2P$ lower level at 0.94 μm. The $3p^2D^0$ is populated by about 17% of the neutralizations.

Since the kinetics and scaling characteristics of the $^3He/N_2O/O_2$ and $^3He/N_2O/N_2$ systems are similar, the discussion will center on the oxygen system. Computed data for the nitrogen system, though, will be shown for comparison. In the following discussion, the oxygen laser line was chosen to be $3p^3P_1$-$3s^3S_1^0$(0.8449 μm), while the nitrogen line is $3p^2D_{3/2}^0$-$3s^2P_{3/2}$(0.9463 μm).

A typical example of the number densities of various species during nuclear pumped excitation in a $^3He/N_2O/O_2$ mixture is shown in Fig. 6. The peak thermal neutron flux is 5×10^{16}(cm^2 s)$^{-1}$. The total initial number density is 1.32×10^{19} cm^{-3} at 1000 °K and with a $^3He/N_2O/O_2$ ratio of 400/0.5/10. The thermal electron density is maximum near the peak of the neutron pulse with a value of 1.3×10^{12} cm^{-3}. The nonthermal electron density has a peak value of 3.7×10^8 cm^{-3}. Neutral species, which result from neutral gas phase reactions, gradually approach new equilibrium values (e.g., NO_2, NO, O_3). The nuclear excitation supplies an activation energy which produces a variety of radicals (e.g., O, N, O^-, N^+). The redistribution of these radicals provides the new equilibrium composition.

The dominant positive ions are N_2O^+, O^+, O_2^+, and He^+. The helium ions result almost exclusively from electron impact excitation and secondarily from fission fragment excitation, the ratio of the ionization rates being 10^6. The remaining atomic and diatomic ions result primarily from charge exchange with He^+, and secondarily from direct electron impact excitation. The chain of charge exchange reactions proceeds, depeleting ions with higher ionization potentials, and results in N_2O^+ being the most abundant positive ion.

The initially large N_2 density is a result of dissociative

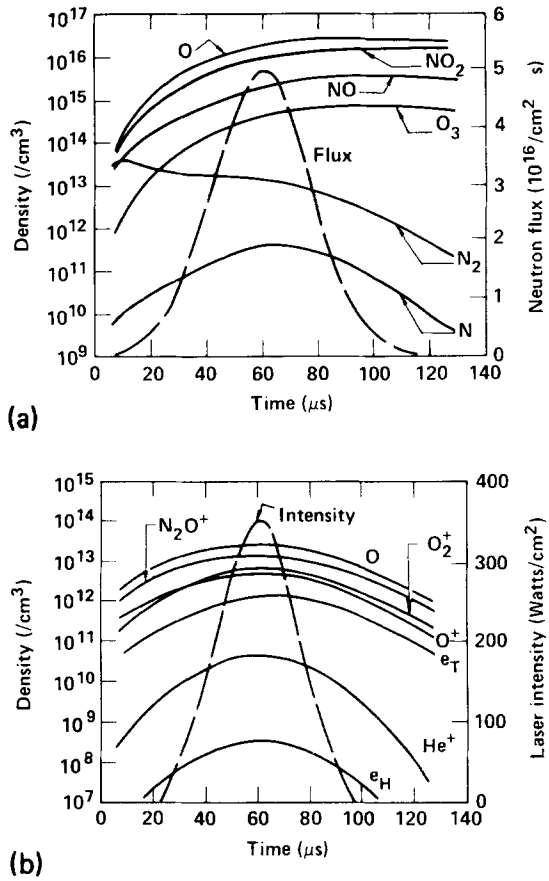

FIG. 6. Typical densities during nuclear excitation of a $^3He/O_2/N_2O = 400/10/0.5$ gas mixture with a peak neutron flux of 5×10^{16} (cm^2 s)$^{-1}$. Total gas density is 1.35×10^{19} cm^{-3} at 1000 °K. (a) Neutral species and neutron flux. (b) Charged species and laser pulse. e_T denotes thermal group electrons and e_H denotes nonthermal electrons.

attachment to N_2O. As N_2O is depleted (by a factor of 2 during the pulse) the N_2 density decreases, lost primarily by charge exchange and neutral reactions which produce NO. NO_2 and NO are the most abundant products. NO is most rapidly produced by electron detachment of O^- by N_2O and N. NO_2 can be considered a terminal species in the reaction chain, being quickly formed from NO by the reactions $O + NO + M \rightarrow NO_2 + M$ and $NO + O_2 \rightarrow NO_2 + O$, the latter being more productive by a factor of about 50.

Reactions which reduce the density of O^-, with the exception of the neutralization collision which populates the upper laser level, can be considered quenching reactions. The total rate of reactions which are quenching is more than twenty times the pumping rate. The quenching reactions primarily responsible for this are O^--O^+ neutralizations which populate the oxygen ground state, electron detachment collisions with O and O_2, forming O_2 and O_3, respectively, and electron detachment by N_2O forming two NO molecules. The last reaction is responsible for the rapid production of NO and has the largest quenching rate.

In the examples which follow, the length of the laser medium is 200 cm with a parasitic loss of 0.04 per pass. Unless noted otherwise, the resonator consists of a 95% reflectivity output coupler and a 100% reflector. The width of

the neutron pulse is 100 μs and the helium pressure is 400 Torr (at 300 °K). The last constraint was chosen in order to obtain uniform excitation over a reasonably large diameter ($\approx$10 cm).

Maximum laser power as function of peak neutron flux is shown in Fig. 7. The gas mixtures are 400/3.1/10 for both $^3He/N_2O/O_2$ and $^3He/N_2O/N_2$ and the gas temperature is 1000 °K. For these conditions, the threshold thermal neutron flux for the oxygen and nitrogen systems is 2.3×10^{15} $(cm^2\ s)^{-1}$ and 3.6×10^{16} $(cm^2\ s)^{-1}$, respectively. Assuming uniform excitation over a 10-cm-diam reaction cell, the quasi-CW power in the oxygen system is 21 kW with $\Phi_{max} = 10^{17}(cm^2\ s)^{-1}$. One of the limiting constraints at high pump power (high neutron fluxes) is depletion of N_2O.

Threshold neutron fluxes for volumetrically pumped systems have experimentally found to be typically a few times 10^{15} $(cm^2\ s)^{-1}$. The lowest threshold flux for lasing reported is believed to be 3×10^{14} $(cm^2\ s)^{-1}$ for oscillation in Cd vapor pumped by the ^3He $(n,p)T$ reaction.[29] A threshold value of 2×10^{11} $(cm^2\ s)^{-1}$ has been reported for the 6328-Å line in neon in a ^{3}He-Ne system,[30] but this value has been disputed.[31] By relaxing the constraint for uniform excitation, increasing the helium pressure, and decreasing the diameter of the reaction cell, the threshold neutron flux in the oxygen system could be reduced by another factor of 2 or 3 to a value near or below 1×10^{15} $(cm^2\ s)^{-1}$. The efficiency of the system, though, would not increase.

In previous sections, we discussed the temperature dependence of the dissociative attachment rate and that of the neutralization rate. The former increases at a faster rate as the gas temperature increases than the latter decreases. The net effect is that the effective pumping rate [i.e., (attachment rate)$\times$(neutralization rate)] increases as the gas temperature is raised. This is illustrated in Fig. 8. The peak neutron flux is

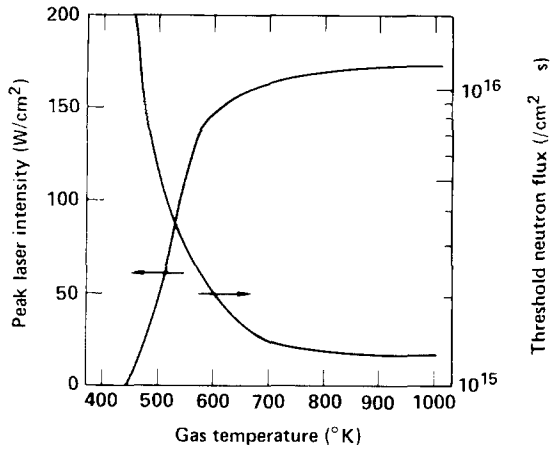

FIG. 8. Maximum laser power and threshold neutron flux for the oxygen system as a function of gas temperature (constant number density). The peak thermal neutron flux is 5×10^{16} $(cm^2\ s)^{-1}$. The threshold gas temperature can be reduced by increasing the peak neutron flux.

5×10^{16} $(cm^2\ s)^{-1}$. Laser power increases significantly as the gas temperature increases. The change in slope of the curves is a result of the change in activation energy of the attachment process near 600 °K. The threshold neutron flux increases with decreasing temperature (see Fig. 8). Room temperature operation could be achieved for sufficiently ciently high fluxes [$\gtrsim 10^{17}$ $(cm^2\ s)^{-1}$].

There is an optimum partial pressure of oxygen, the value of which is determined by a variety of causes. By increasing the partial pressure of O_2, the fraction of energy deposited in oxygen relative to the helium increases. The fraction of these impact processes which produce positive atomic oxygen ions (required for the pumping process) is small compared to those that produce molecular oxygen ions. Charge exchange of O_2 with helium ions form O^+ and O_2^+ in about the same proportions. Therefore, increasing the partial pressure of oxygen beyond that required to insure that He_2^+ ions are not rapidly formed by termolecular colli-

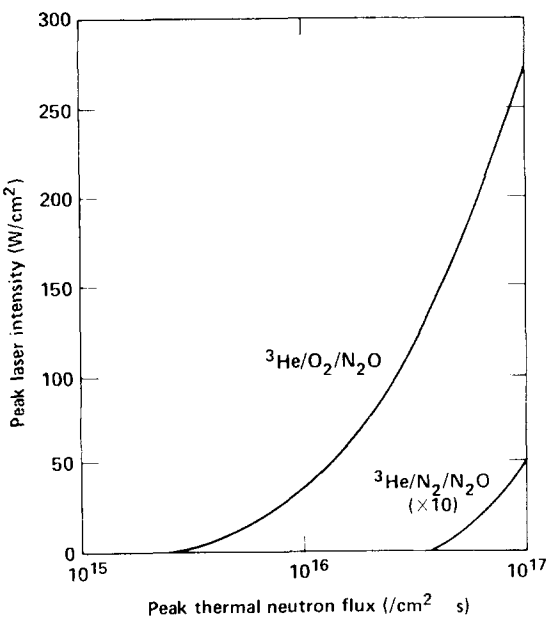

FIG. 7. Maximum laser intensity as a function of peak thermal neutron flux during a 100-μs-long neutron pulse. Threshold flux in the oxygen system is $\approx2\times10^{15}$ $(cm^2\ s)^{-1}$, and in the nitrogen system is $\approx3\times10^{16}$ $(cm^2\ s)^{-1}$.

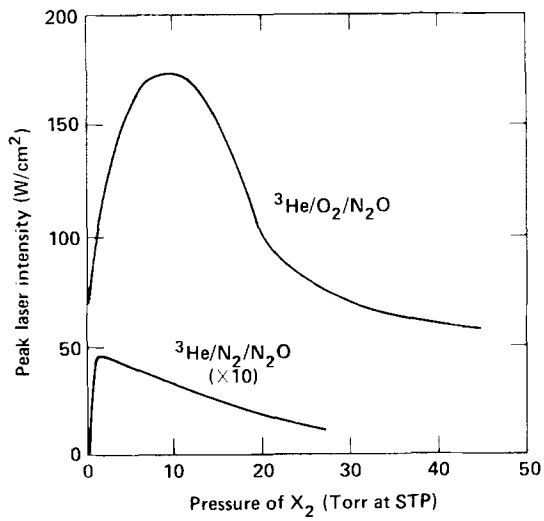

FIG. 9. Maximum laser power as a function of the partial pressure of N_2 and O_2. The decrease in laser power with increasing pressure of O_2 and N_2 is due to formation of molecular ions and detachment collisions with O^-.

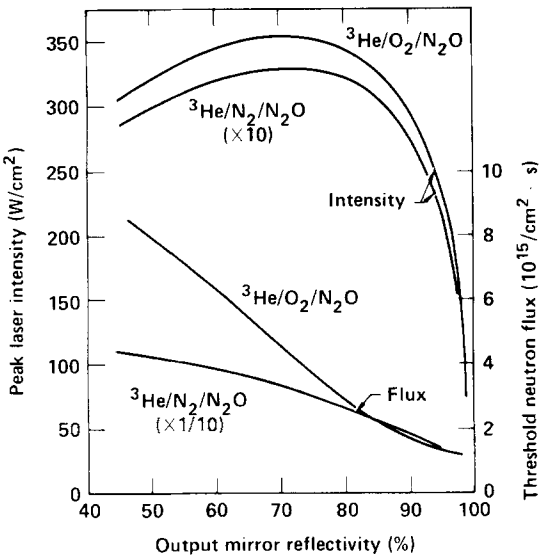

FIG. 10. Maximum laser intensity and threshold neutron flux as a function of output mirror reflectivity. Total number density is 1.35×10^{19} cm^{-3} at 1000 K. The gas mixtures are $^3He/O_2/N_2O = 400/10/0.5$ and $^3He/N_2/N_2O = 400/5/0.5$.

sions with ground-state helium can actually decrease the density of atomic oxygen ions. In addition, detachment collisions of O^- by O_2 are a dominant quenching mechanism. Although negative oxygen ions can be formed by dissociative attachment collisions of O_2 by electrons and direct attachment to atomic oxygen, these rates are small compared to dissociative attachment to N_2O. Therefore, increasing the O_2 partial pressure to create O^- in this manner gains little.

Laser power as a function of the partial pressure of O_2 (and N_2) is shown in Fig. 9. The optimum oxygen pressure is near 10 Torr, while the optimum nitrogen pressure is about 1 Torr. The lower optimum nitrogen pressure is due in large part to the rapid termolecular collisional detachment of O^- by N_2. This rate is equal to the neutralization rate of N^+ and O^- at a nitrogen pressure of only a few Torr. Note that laser oscillation is predicted in atomic oxygen in $^3He/N_2O$ mixtures. The source of positive oxygen ions is principally dissociative charge exchange of N_2O by He^+, and charge exchange of atomic oxygen by He^+. The source of atomic oxygen is principally dissociative attachment of electrons to N_2O and subsequent neutralization of O^-.

Laser output power as a function of output mirror reflectivity is shown in Fig. 10. For both the oxygen and nitrogen systems, optimum laser power is obtained for reflectivities from 0.7 to 0.8. As the output mirror reflectivity decreases, the threshold neutron flux increases. At near optimum conditions, the threshold neutron flux in the oxygen system is 5×10^{15} (cm^2 s)$^{-1}$ while that for nitrogen is 3×10^{16} (cm^2 s)$^{-1}$.

For the near optimum conditions previously described ($^3He/N_2O/O_2 = 400/0.5/10$, gas temperature = 1000 °K, gas density = 1.3×10^{19} cm^{-3}), the maximum laser output power for a peak neutron flux of 10^{17} (cm^2 s)$^{-1}$ is predicted to be more than 520 W/cm^2. Assuming uniform excitation over an active region 10 cm in diameter, total laser power is 41 KW. The fission power to laser power conversion efficiency for these conditions is 0.3%.

VI. CONCLUDING REMARKS

A nuclear pumped laser has been described whose excitation mechanism is ion-ion neutralization. This process is highly selective in terms of the product-excited states which are populated, and therefore has many advantages over electron-ion recombination NPL. In mixtures of $^3He/N_2O/O_2$, near-ir laser oscillation is predicted in excess of 500 W/cm^2 under optimum conditions. Steady-state operation is limited by the depletion of N_2O. A flowing system would be required for cw operation.

[1]R. J. DeYoung and F. Hohl, IEEE J. Quantum Electron. **QE-16**, 1114–1117 (1980).
[2]D. A. McArthur and P. B. Tollefsrud, Appl. Phys. Lett. **26**, 187–190 (1975).
[3]R. J. DeYoung, N. W. Jalufka, and F. Hohl, Appl. Phys. Lett. **30**, 19–21 (1977).
[4]M. A. Prelas, M. A. Akerman, F. P. Boody, and G. H. Miley, Appl. Phys. Lett. **31**, 428–430 (1977).
[5]H. H. Helmick, J. L. Fuller, and R. T. Schneider, Appl. Phys. Lett. **26**, 327–328 (1975).
[6]F. P. Boody, M. A. Prelas, J. H. Anderson, S. J. S. Nagalingam, and G. H. Miley, Prog. Astronaut. Aeronaut. **61**, 379–410 (1978).
[7]J. W. Wilson, R. J. DeYoung, and W. L. Harries, J. Appl. Phys. **50**, 1226–1235 (1979).
[8]J. E. Deese and H. A. Hassan, AIAA 16th Aerospace Sciences Meeting, Paper 78-69, 1978.
[9]R. H. Lo and G. H. Miley, IEEE Trans. Plasma Sci. **PS-2**, 198–205 (1974).
[10]H. A. Hassan and J. E. Desse, Phys. Fluids **19**, 2005–2011 (1976).
[11]R. E. Olson, J. R. Peterson, and J. Moseley, J. Chem. Phys. **53**, 3391–3397 (1970).
[12]R. E. Olson, F. T. Smith, and E. Bauer, Appl. Opt. **10**, 1848–1854 (1971).
[13]P. J. Chantry, J. Chem. Phys. **51**, 3369–3379 (1969).
[14]H. Shimamori and R. W. Fessenden, J. Chem. Phys. **70**, 1137–1141 (1979).
[15]B. M. Smirnov, Sov. Phys. Dokl. **12**, 242–244 (1967).
[16]C. H. Brau, in *Excimer Lasers*, edited by Ch. K. Rhodes (Springer-Verlage, Berlin, 1979), pp. 87–133.
[17]M. Gryzinski, Phys. Rev. A **138**, 336–358 (1965).
[18]W. L. Morgan, JILA Information Center Report No. 19, University of Colorado, 1979.
[19]S. D. Rockwood, Phys. Rev. A **8**, 2348–2358 (1973).
[20]C. J. Elliot and A. E. Greene, J. Appl. Phys. **47**, 2946–2953 (1976).
[21]C. B. Opal, E. C. Beatly, and W. K. Peterson, At. Data **4**, 204–253 (1972).
[22]A. E. S. Green and T. Sawada, J. Atmos. Terr. Phys. **34**, 1719–1728 (1972).
[23]D. Rapp and D. Briglia, J. Chem. Phys. **43**, 1480–1489 (1965).
[24]L. E. Kline, D. K. Davies, C. L. Chen, and P. J. Chantry, J. Appl. Phys. **50**, 6789–6796 (1979).
[25]H. L. Chen, R. E. Center, D. W. Trainor, and W. I. Fyfe, Appl. Phys. Lett. **30**, 99–101 (1977).
[26]C. K. N. Patel, R. A. McFarlane, and W. L. Faust, Phys. Rev. A **133**, 1244–1248 (1964).
[27]R. J. DeYoung, W. E. Wells, and G. H. Miley, Appl. Phys. Lett. **28**, 194–197 (1976).
[28]M. S. Feld, B. J. Fledman, and A. Javan, Phys. Rev. A. **7**, 257–269 (1973).
[29]A. I. Mis'kevich, A. B. Dmitriev, V. S. Ii'yashchenko, B. S. Salamakha, V. A. Stepanov, and E. M. Gorodkov, Sov. Tech. Phys. Lett. **6**, 352–353 (1980).
[30]B. D. Carter, M. J. Rowe, and R. T. Schneider, Appl. Phys. Lett. **36**, 115–117 (1980).
[31]M. A. Prelas and G. A. Schlapper, J. Appl. Phys. **52**, 496–497 (1981); R. T. Schneider, B. D. Carter and M. J. Rowe, J. Appl. Phys. **52**, 6980 (1981).